Defense Technical Information Center
Compilation Part Notice

ADP011040

TITLE: Purpose-Built Anisotropic Metal Oxide Nanomaterials

DISTRIBUTION: Approved for public release, distribution unlimited

This paper is part of the following report:

TITLE: Materials Research Society Symposium Proceedings Volume 635. Anisotropic Nanoparticles - Synthesis, Characterization and Applications

To order the complete compilation report, use: ADA395000

The component part is provided here to allow users access to individually authored sections of proceedings, annals, symposia, etc. However, the component should be considered within the context of the overall compilation report and not as a stand-alone technical report.

The following component part numbers comprise the compilation report:
ADP011010 thru ADP011040

Purpose-Built Anisotropic Metal Oxide Nanomaterials

Lionel Vayssieres, Jinghua Guo and Joseph Nordgren
Department of Physics, Uppsala University, Box 530, SE-75121 Uppsala, Sweden

ABSTRACT

Large arrays of perpendicularly oriented anisotropic nanoparticles of ferric oxyhydroxide (Akaganeite, β-FeOOH) and oxide (Hematite, α-Fe$_2$O$_3$) of typically 3-5 nm in diameter, self-assembled as bundles of about 50 nm in diameter and of up to 1 μm in length have been successfully grown onto polycrystalline substrates without template and/or surfactant by heteronucleation from an aqueous solution of ferric salts and their optical and electronic properties investigated.

INTRODUCTION

Iron compounds are essential materials in chemistry, biology and geology due to their large occurrence in nature [1], for instance, in water [2], plants [3], minerals [4] and clay minerals [5], sediments [6], and sedimentary rocks [7]. The molten core of the Earth is primarily elemental iron, which is the fourth most abundant element in the Earth's crust and is found in significant amount in Martian soil [8]. The oxides of iron play a central role in geochemistry of soil [9], in planetary science [10], and contribute for instance, to the oxidation of sedimentary organic matter [11]. In its various allotropic forms, iron oxides and oxyhydroxides represent important basic and raw materials [12]. Their large abundance, non-toxicity, low-cost, high refractivity, and various colors, contribute to their popularity as polishing agents, and for colorants (red and yellow ochre) for the pigment and paint industry. Indeed, iron oxides are the most commonly used colored pigments in the paints and coatings market [13]. It is also widely studied for the alloys and steel industry [14], in metallurgy [15], as catalysts [16-18] and photocatalysts [19], for magnetic storage devices, cathodes for primary and secondary batteries [20], chemical flame suppressant [21] and for the crucial industrial, economical and environmental issue of corrosion [22]. The thermodynamically stable crystallographic phase of ferric oxides is hematite (α-Fe$_2$O$_3$) which represents the most important ore of iron considering its high iron content and its natural abundance. Therefore, designing iron(III) oxides with a novel, anisotropic and highly oriented morphology is of great fundamental importance for basic physical, earth and life sciences and of relevance for various fields of industrial applications. Numerous vacuum deposition techniques have been used to generate thin films of iron oxides (e.g. molecular beam epitaxy [23], chemical vapor deposition [24], cathodic sputtering [25], and metal deposition and subsequent oxidation [26]). Our strategy is a chemical approach and a general concept named "*purpose-built materials*" [27], well-sustained by a thermodynamic monitoring of the nucleation, growth and ageing processes [28] and well-illustrated on the nanoparticle size control of magnetite (Fe$_3$O$_4$) over an order of magnitude [29]. This concept and synthetic method allows to design and create novel metal oxide nanomaterials with the proper morphology, texture and orientation in order to probe, tune, and optimize their physical properties. Thin films materials are obtained by direct growth onto various substrates from aqueous precursors at low temperature. Such approach to material synthesis offers the ability to generate anisotropic nanoparticles as well as the competence to control their orientation on substrates.

EXPERIMENTAL

The general concept [27] and synthetic procedure is performed according to the general template-less thin film processing technique developed by Vayssieres et al. [30] and has been successfully applied for the growth of large arrays of highly oriented anisotropic metal oxides [31, 32]. Iron(III) oxides thin films (akaganeite and hematite) are grown directly onto a substrate from aqueous ferric chloride salt at 95°C in such conditions that the thermodynamic stabilization of the oxyhydroxide structure (akaganeite) is obtained [31]. A subsequent heat treatment in air is performed to obtain monodisperse nanorod-array of hematite. The solid phase transition was followed by thermal analysis (i.e. differential scanning calorimetry (DSC) and thermogravimetric analysis (TGA) performed in air at a heating rate of 10°C/min. The electronic structure was investigated by soft x-ray absorption spectroscopy (XAS) at synchrotron facilities (Advanced Light Source, Lawrence Berkeley National Laboratory, BL 7.0.1).

RESULTS AND DISCUSSION

β-FeOOH occurs in nature as the mineral akaganeite and crystallizes in the tetragonal system (space group $I4/m \equiv C_{4h}^5$, a = 10.44, c = 3.01 Å). The structure is described as a tunnel structure (similar to α-MnO$_2$) hosting H$_2$O or Cl$^-$ and based on a defect close packed oxygen lattice with three different kinds of oxygen layers. Every third layer is only two-third occupied with rows of oxygens missing along the c-axis. The cation occupation of octahedral sites between the other anion layers is in double rows, but separated by single rows of empty sites along c. The octahedral cation sites remain between the third anion layer and its neighbor layer are completely filled. This topology produces di-octahedral chains, which are arranged about the four-fold symmetry c-axis (figure 1). The chains share vertices along their edges, forming square-cross section tunnels, some 5 Å on edge. Although, the tunnel seems large it must be noted that only a single row of oxygens is missing. Hence, only species with sizes similar to O$_2^-$ ions can be readily accommodated. The crystals are rod shaped grouping of 5*5*n unit cells where n refers to replication down the c-axis. These crystals have empty cores, that is, 3*3*n cell hole runs down the center of the crystal, producing a square channel about 3 nm on a side. The anisotropic crystals form a bundle called a somatoid. Dehydration of β-FeOOH at high temperature leads to the thermodynamically stable α-Fe$_2$O$_3$ phase.
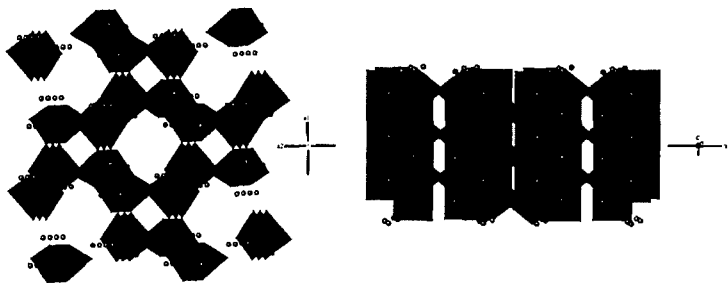

Figure 1. *Crystal structure of β-FeOOH (akaganeite). The spheres represent hydrogen atoms.*
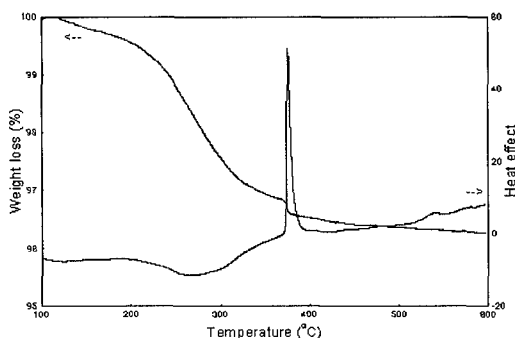
Figure 2. TGA (left scale) and DSC (right scale) analysis of β-FeOOH nanorod powder.

Thermal analysis of β-FeOOH nanorods (figure 2) shows a low overall weight loss of 3.75% within the range of 100-600° C. A 0.5% loss due weakly bonded water molecules occurs until 200°C. Most of the weight loss (3%) is occurring between 200 and 300°C accompanied by a broad endothermic shoulder which corresponds to the evaporation of structural water. A very sharp exothermic peak occurs at 385°C with a concomitant 0.2% loss of water corresponding to the crystal phase transition to hematite. A continuous slow decay of the TGA curve is observed until 600°C corresponding to the slow process of diffusion and evaporation of surface/bulk OH groups as H_2O with a very small exothermic peak at 540°C.

Hematite crystallizes in the trigonal crystal system, space group $R\overline{3}c \equiv D_{3d}^6$, and is isostructural with corundum (α-Al_2O_3). The unit cell can be described as rhombohedral with three equal axes a = 5.43 Å and an angle between edges α = 55°18' containing two formula unit (Z = 2), or hexagonal with a = 5.03Å and c = 13.75 Å (Z = 6). The lattice is built on a hexagonal close packed (HCP) array of oxygen with four of every six available octahedral sites around O atoms occupied with Fe (figure 3). The octahedral and tetrahedral sites are above and below one another in a HCP lattice, the tetrahedral sites remaining empty. Octahedra are sharing faces along a threefold axis and are distorted to trigonal antiprisms because of the Fe-Fe repulsion occurring across one shared face and not the others. This yields to a very dense structure (i.e. high oxygen packing index), showing a high polarisability and a high refractive index.
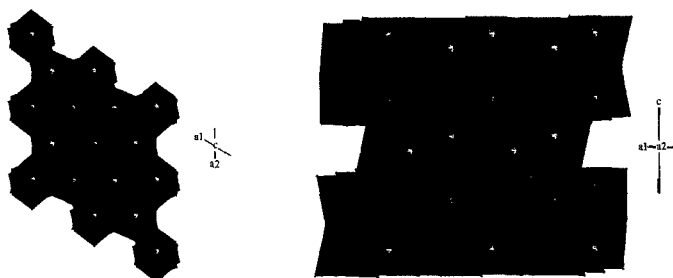

*Figure 3. Crystal structure of α-Fe_2O_3 (hematite).*
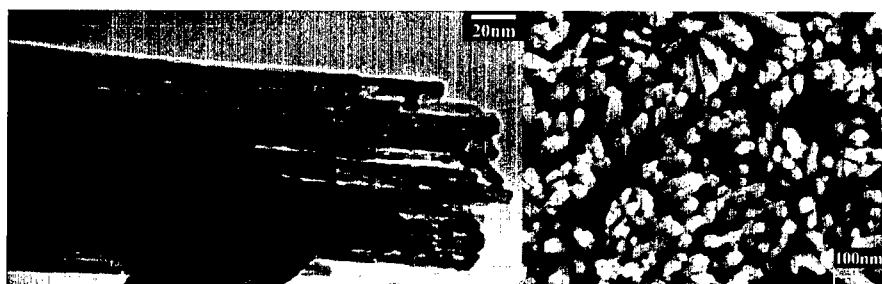
Figure 4. *(left) TEM of α-Fe₂O₃ somatoid and (right) SEM of α-Fe₂O₃ oriented nanorod-array.*

The purpose-built nanorod-array, consisting in a somatoid of about 50 nm in diameter with single-crystalline nanorods of 3-5 nm in diameter, perpendicularly oriented onto the substrate is shown on figure 4. Figure 5 shows the x-ray absorption spectra (XAS) of hematite nanorod-array at Fe L-edge and O K-edge. The Fe L-edge (2p → 3d) spectrum shows the spin orbit splitting of the 2p core level, i.e. $2p_{3/2}$ (L₃-edge) and $2p_{1/2}$ (L₂-edge) and the p-d and d-d coulomb and exchange interactions that create multiplet feature within the edge. The ligand field splitting of 3d transition metals being in the same order of magnitude than p-d and d-d interactions, the energy splitting between t_{2g} and e_g orbitals of the Fe^{3+} ion (d^5) in distorted octahedral symmetry is found to be of 1.4 eV. The oxygen K-edge spectrum (1s → 2p) shows two regions corresponding to oxygen 2p orbitals hybridized respectively, with Fe 3d orbitals (530-535 eV) and with Fe 4s,4p orbitals (535-550 eV).

The UV visible properties of the hematite nanorod-array are shown on figure 6. A strong optical absorption in the UV and visible (blue) region (350-550 nm) is found, which spread out, to a lower extent, into the entire visible region. This broad absorption and good stability against photocorrosion (Eg ≈ 2.2 eV) has driven much efforts in the past to produce photovoltaic cells from n-type hematite materials but very unsuccessfully, due to a high and fast rate of recombination of photogenerated carriers and a low carrier mobility. Thin films of nanostructured hematite based on spherical nanoparticles of 50 nm have been synthesized in an attempt to reduce the charge recombination but the efficiency remained very low [33].
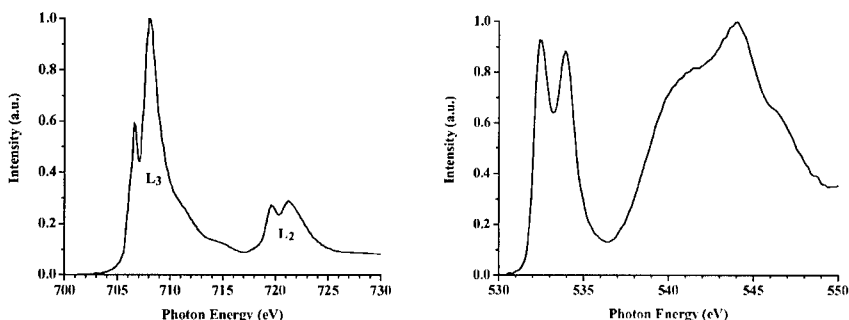
Figure 5. *XAS spectra at Fe L-edge (left) and O K-edge (right) of α-Fe₂O₃ nanorod-array.*
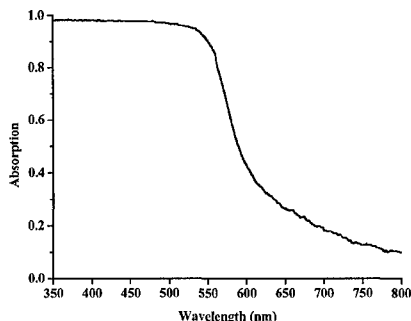
Figure 6. UV-Visible optical absorption spectrum of hematite nanorod-array.

Recently, such *purpose-built* perpendicularly oriented nanorod-arrays of hematite have been used to develop photovoltaic cells. Indeed, the diameter of the nanorods allows a perfect match with the minority carrier diffusion length of hematite [34]. Accordingly, a very efficient photogenerated charge separation was obtained as well as a high incident photon to electron conversion efficiency of ca. 60% at 350 nm, which led to the creation of a 2-electrode hematite photovoltaic cells [35]. Besides the well-designed direct, grain boundary-free, electron pathway and the excellent structural match with the hole diffusion length, a 2D quantum confinement has also been suggested from resonant inelastic x-ray scattering (RIXS) of synchrotron radiation [36] to account for the unusual high efficiency of the hematite nanorod-array photoanode.

Such design is suitable for other oxides and allowed, for instance, the creation of highly oriented arrays of ZnO [32] to study the photoelectrochemical, electron transport, and luminescence properties as well as to probe and demonstrate the character and symmetry of ZnO conduction band orbitals by polarization-dependent x-ray absorption spectroscopy and quantum calculation study [37].

CONCLUSION

The ability to produce, at low cost, anisotropic nanoparticles and to control their orientation onto a substrate in order to generate well-controlled 3D nanostructures, will contribute to create a novel generation of smart and functional nanomaterials, built for the purpose of their applications: the materials of the future. Simultaneously, it should contribute to reach a better fundamental understanding of their fascinating physical properties and therefore, bring the competence to optimize existing devices and, most probably, developing new ones.

ACKNOWLEDGEMENTS

REFERENCES

1. J. L. Jambor and J. E. Dutrizac, *Chem. Rev.* **98**, 2549-2585 (1998).

2. W. Stumn and J.J. Morgan, *Aquatic Chemistry* (Wiley, 1996).
3. G. Winklemann, F. Van der helm and J. B. Neidlans, *Iron transport in Microbes, Plants and Animals* (VCH, 1987).
4. L. A. J. Garvie and P. R. Buseck, *Nature* **396**, 667-670 (1998).
5. J. E. Kostka, E. Haefele, R. Viehweger and J.W. Stuck, *Environ. Sci. Technol.* **33**, 3127-3133 (1999).
6. H. M. Bao, P. L. Koch and R. P. Hepple, *J. Sediment. Res.* **68(5)**, 727-738 (1998).
7. B. B. Ellwood, K. M. Petruso, F. B. Harrold and D. Schuldenrein, *J. Archeological Sci.* **24**, 569-573 (1997).
8. R.V. Morris, D.C. Golden, T.D. Shelter and H.V. Lauer, *Meteorit. Planet. Sci.* **33(4)**, 743-751 (1998).
9. W. Stumm and B. Sulzberger, *Geochim. Cosmochim. Acta* **56(8)**, 3233-3257 (1992).
10. G. Kletetschka, P. Wasilewski and P. Taylor, *Phys. Earth Planet. In.* **119**, 259-267 (2000).
11. D. R. Lovley, *Microbiol. Rev.* **55(2)**, 259-287 (1991).
12. R. M. Cornell and U. Schwertmann, *The Iron Oxides* (VCH, 1996).
13. P. G. Morse, *Chem. Eng. News* **76(41)**, 42-62 (1998).
14. K. Tano, E. Öberg, P. O. Samskog, T. Monredon and A. Broussaud, *Powder Technol.* **105**, 443-450 (1999).
15. A. Von Ropenack, in J.E. Dutrizac and A.J. Monhemius Eds. *Iron control in Hydrometallurgy* (Ellis Horwood, 1986) pp. 730-741.
16. R. Pestman, R.M. Koster, E. Boellaard, A.M. Van der Kraan and V. Ponec, *J. Catal.* **174**, 142-152 (1998).
17. S-S. Lin and M. D. Gurol, *Environ. Sci. Technol.* **32**, 1417-1423 (1998).
18. Y. Zhang, J. E. Ellison and J.C. Cannon, *Ind. Eng. Chem. Res.* **36(5)**, 1948-1952 (1997).
19. Y. Matsumoto, *J. Solid State Chem.* **126**, 227-234 (1996).
20. S. Licht, B. Wang and S. Ghosh, *Science* **285**, 139-1042 (1999).
21. C. B. Kellog, K. K. Irikura, *J. Phys. Chem. A* **103(8)**, 1150-1159 (1999).
22. S. E. Oh, D.C. Cook and H.E. Townsend, *Corrosion Sci.* **41**, 1687-1702 (1999).
23. T. Fujii, et al *Surf. Sci.* **366(3)**, 579-586 (1996).
24. A. Martinez, J. Pena, M. Labeau, J.M. Gonzalez-Calbet and M. Vallet-Regi, *J. Mater. Res.* **10(5)**, 1307-1311 (1995).
25. K. Siroky, J. Jiresova and L. Hudec, *Thin Solid Films* **245(1-2)**, 211-214 (1994).
26. W. Weiss, *Surf. Sci.* **377(1-3)**, 943-947 (1997).
27. L. Vayssieres, A. Hagfeldt and S.-E. Lindquist, *Pure Appl. Chem.* **72(1-2)**, 47-52 (2000).
28. L. Vayssieres, Ph.D. Dissertation, Université Pierre et Marie Curie, Paris 1995.
29. L. Vayssieres, C. Chaneac, E. Tronc and J.-P. Jolivet, *J. Colloid Interface Sci.* **205(2)**, 205-212 (1998).
30. L. Vayssieres, A. Hagfeldt, S.-E. Lindquist, patent pending.
31. L. Vayssieres, N. Beermann, S.-E. Lindquist and A. Hagfeldt, *Chem. Mater.* (in press).
32. L. Vayssieres, K. Keis, S.-E. Lindquist and A. Hagfeldt, submitted.
33. U. Björksten, J. Moser and M. Grätzel, *Chem. Mater.* **6**, 858-863 (1994).
34. J. H. Kennedy and K. W. Frese, *J. Electrochem. Soc.* **125**, 709 (1978).
35. N. Beermann, L. Vayssieres, S.-E. Lindquist and A. Hagfeldt, *J. Electrochem. Soc.* **147(7)**, 2456-2461 (2000).
36. J.-H. Guo, L. Vayssieres, C. Såthe, S. Butorin and J. Nordgren to be published.
37. J.-H. Guo, L. Vayssieres, C. Persson, R. Ahuja, and J. Nordgren to be published.